

THE AFTERGLOW OF MASSIVE BLACK HOLE COALESCENCE

MILOŠ MILOSAVLJEVIĆ¹ AND E. S. PHINNEY¹¹Theoretical Astrophysics, California Institute of Technology, Pasadena, CA 91125, milos,esp@tapir.caltech.edu*Draft version February 7, 2020*

ABSTRACT

The final merger of a pair of massive black holes in a galactic nucleus is compelled by gravitational radiation. Gravitational waves from the mergers of black holes of masses $10^{5-7}(1+z)^{-1}M_{\odot}$ at redshifts of 1–20 will be readily detectable by the Laser Interferometer Space Antenna (LISA), but an electromagnetic afterglow would be helpful in pinpointing the source and its redshift. Long before the merger, the binary “hollows out” any surrounding gas, and shrinks slowly compared to the viscous timescale of a circumbinary disk. The inner gas disk is truncated at the radius where gravitational torque from the binary balances the viscous torque, and accretion onto the black holes is suppressed. Initially the inner truncation radius is able to follow the shrinking binary inwards. But eventually the gravitational radiation timescale becomes shorter than the viscous timescale in the disk, leading to a merged black hole surrounded by a hollow disk of gas. We show that the subsequent viscous evolution of the hollow, radiation-pressure dominated disk will create a $\sim 10^{43.5}(M/10^6M_{\odot})\text{erg s}^{-1}$ X-ray source on a timescale $\sim 7(1+z)(M/10^6M_{\odot})^{1.32}\text{ yr}$. This justifies follow-up monitoring of gravitational wave events with next-generation X-ray observatories. Analysis of the detailed light curve of these afterglows will yield new insights into the subtle physics of accretion onto massive black holes.

Subject headings: accretion, accretion disks — black hole physics — quasars: general — X-rays: galaxies

1. INTRODUCTION

Evidence is mounting that most galactic spheroids contain massive black holes (MBH) in their nuclei. When two galaxies merge, their MBH form a binary in the nucleus of the new galaxy (Begelman, Blandford, & Rees 1980). The binary interacts with its stellar and gaseous environment and with other MBH that can collect in the same nucleus in multiple mergers. These interactions torque the binary and extract its orbital angular momentum and energy. The binary can thus be rendered so compact that gravitational radiation (GR) carries away its remaining orbital energy, inducing coalescence. For binaries with masses $M = M_1 + M_2 \lesssim 10^7M_{\odot}$, the gravitational slingshot ejection of stars by the binary could be sufficient to guarantee coalescence in a Hubble time (Milosavljević & Merritt 2003). GR emitted by these binaries shortly before and during coalescence will be detected by the space-based gravitational wave detector *Laser Interferometer Space Antenna* (LISA)¹. The coalescence of isolated black holes in general relativity is not accompanied by observable electromagnetic emission. We here show that circumbinary gas can lead to a delayed electromagnetic afterglow.

Of interest to LISA are mergers of binaries with masses $M < 10^7M_{\odot}$ of arbitrary mass ratio $q \leq 1$. Observations offer abundant evidence for dense gas in galactic nuclei. Geometrically thin molecular disks at radii $\sim (0.1 - 0.5)\text{ pc}$ have been observed in water maser emission in Seyferts (e.g., Miyoshi et al. 1995; Greenhill et al. 2003). The Galactic nucleus contains a $4 \times 10^6M_{\odot}$ MBH surrounded by a $\sim 10^4M_{\odot}$ molecular gas torus at radii $\gtrsim 1\text{ pc}$ (e.g., Jackson et al. 1993). Massive accretion disks must be present in quasars and narrow-line Seyfert I nuclei to account for the fueling of the central engine.

In general the specific angular momentum of inflowing gas exceeds that of the binary, while the gas temperature is below the virial temperature $GM\mu m_p/2ak$ associated with the binary’s orbit, where μ is the mean molecular weight in units

of the proton mass m_p , a is the binary’s semimajor axis, and k is the Boltzmann constant. The sub-virial gas cools and settles into a rotationally-supported, geometrically-thin circumbinary disk. If the disk is inclined with respect to the binary’s orbital plane, the quadrupole component of the binary’s gravitational potential causes differential precession and the warping of the disk. As in the Bardeen & Petterson (1975) mechanism, the warp dissipates viscously, resulting in a disk in the binary’s orbital plane (Larwood & Papaloizou 1997; Ivanov, Papaloizou, & Polnarev 1999).

The disk is truncated at an inner edge where gravitational torques and viscous stresses balance (Artymowicz & Lubow 1994). Angular momentum transfer from the binary to the disk can involve excitation and damping of density waves and tides. Since little gas accretes across the circumbinary gap (Armitage & Natarajan 2002; but see Artymowicz & Lubow 1996), the disk is confined in a quasi-steady configuration. As the binary’s semimajor axis decays due to stellar or gas-dynamical processes (including angular momentum extraction by the circumbinary disk itself), the disk’s inner edge spreads inward viscously while maintaining an approximately constant ratio of inner edge radius to semimajor axis ratio, $r_{\text{edge}}/a \sim 2$. In the final stages of in-spiral, however, the time for decay of the relative semimajor axis a is set by gravitational radiation and decreases rapidly with a (equation 1). When this becomes shorter than the (viscous) time for the inner edge of the disk to spread inward, the binary continues toward merger while the disk structure remains frozen.

Vertical support in the central parts of MBH accretion disks is dominated by radiation pressure, while opacity is dominated by electron scattering. The Shakura & Sunyaev (1973) α -disks in this regime are thermally and viscously unstable (Lightman & Eardley 1974) if viscous stresses scale with total pressure. However, they are stable if the stresses scale with the gas pressure alone (Sakimoto & Coroniti 1981). Such a scaling can occur (Turner 2004) if the distance photons diffuse per orbit is about equal to the scale of magnetic fields produced by the magnetorotational instability (MRI;

¹ <http://lisa.jpl.nasa.gov>

Balbus & Hawley 1991), which are being for the angular momentum transport. The radiation then partly decouples from the turbulence driven by the MRI (Turner et al. 2003). These disks are clumpy and porous to the radiation produced within (Begelman 2002 and references therein).

We here describe the observable signatures of such circumbinary disks in MBHs. In § 2 we present a scenario for the combined evolution of a MBH binary and its circumbinary accretion disk during the brief period preceding coalescence. In § 3 we discuss observable signatures.

2. A MODEL FOR BINARY-DISK EVOLUTION

In the early stages of the GR-driven orbital evolution, the binary orbit is circularized by GR. Furthermore, unless $q \ll 1$, the time scale (Peters 1964)

$$t_{\text{gr}} \equiv \frac{a}{da/dt} = \frac{5}{64} \frac{c^5 a^4}{G^3 M^3} \frac{(1+q)^2}{q}. \quad (1)$$

on which the binary's semimajor axis a decays due to the emission of GR greatly *exceeds* the viscous time scale $t_{\text{visc}} = (2/3)r^2/\nu(r)$ for $r \sim a$. For realistic disks (see below), the effective kinematic viscosity ν is a weak function of radius, so $t_{\text{visc}} \propto r^2$ approximately. Thus any gas *inside* the binary orbit should long ago have been accreted (for $r \ll a$) or expelled (for $r \sim a$), leaving the MBHs in a gas-free, “donut hole.”²

Gas outside the binary will attempt to accrete, but be prevented by torques from the binary (§ 1). The inner edge of the disk lies at $r_{\text{edge}} = 2\lambda a$, where $\lambda > 0.5$ is a parameter of order unity. In this regime the viscous torque in the disk $3\pi r^2 \nu \Sigma \Omega^2$ is constant with radius. Here, Σ is the surface density and $\Omega = (GM/r^3)^{1/2}$ is the local angular velocity of the disk. As the binary shrinks, the inner parts of the circumbinary disk pass through a time sequence of non-accreting, constant torque configurations. In the outer parts of the disk it can occur that $t_{\text{gr}} < t_{\text{visc}}(r)$, where r is a radius in the disk. Then material outside r loses viscous causal connection with the boundary condition at the inner edge and decouples from the binary torque.

Since $t_{\text{gr}} \propto a^4$, while the viscous time scale at r_{edge} approximately scales as $t_{\text{visc}} \propto a^2$, the shrinking binary/disk system eventually reaches a state in which $t_{\text{gr}} < t_{\text{visc}}(r_{\text{edge}})$, i.e., the whole disk has decoupled from the rapidly shrinking binary. The inner parts of the disk begin to evolve as a standard, zero-torque disk. When the inner edge decouples, the radial profile closely resembles the non-accreting disk with a fairly sharp edge. Numerical simulations (Milosavljević et al. 2004, in preparation) suggest $(d \ln \Sigma / d \ln r)^{-1} \sim 0.1$ near the edge.

The time for the inner edge to reach the center is

$$t_{\text{sh}} \sim \beta t_{\text{visc}}(r_{\text{edge}}), \quad (2)$$

where $\beta \equiv \max\{0.1, [d \ln \Sigma / d \ln r(r_{\text{edge}})]^{-1}\}$. The factor 0.1 is appropriate for an infinitely sharp disk (Lynden-Bell & Pringle 1974). In order to estimate t_{sh} and the self-consistent a for which $t_{\text{gr}} \sim t_{\text{sh}}$, we must determine the internal structure and viscosity of the inner disk at the time of decoupling, to which problem we turn now.

In the stable α -model the kinematic viscosity is given by $\nu \sim (2/3)\alpha_{\text{gas}} P_{\text{gas}} / \rho \Omega$, where $P_{\text{gas}} = \rho kT / \mu m_p$ is the gas pressure, and ρ is the density. To prevent confusion we have defined α_{gas} , related to the usual definition via $\alpha_{\text{gas}} P_{\text{gas}} = \alpha P_{\text{total}}$,

² This is in contrast to the $q \ll 1$ case considered by Armitage & Natarajan (2002), who assumed that there was still gas accreting onto the black holes.

where $P_{\text{total}} = P_{\text{rad}} + P_{\text{gas}} + P_{\text{mag}}$ is the sum of the radiation, gas, and magnetic pressures. For example, in a simulation of one such accretion disk Turner (2004) measures $\alpha = 0.0013$ and $P_{\text{rad}}/P_{\text{gas}} = 14$ while $P_{\text{mag}} \ll P_{\text{rad}}$, implying that $\alpha_{\text{gas}} \approx 0.02$ in his simulation. We defer modeling the detailed vertical structure of the disk to a follow-up paper; relations presented below are approximate.

The rate of local dissipation per unit area of the disk equals $\mathcal{Q} \sim (9/4)\nu \Sigma \Omega^2$. Ignoring horizontal advection, the flux $F = \mathcal{Q}/2$ must be emitted from each surface. If the surface is emitting as a black body, the flux equals $F_{\text{bb}} = 4\sigma T^4 / 3\tau$, where T is the midplane temperature, τ is the total optical depth of the midplane, and σ is the Stefan-Boltzmann constant. The spectrum differs from that of a black body since the photons at different frequencies are thermalized at different depths in the disk. The modified, “grey-body” spectrum has emergent flux $F_{\nu} \sim \pi \epsilon_{\nu}^{1/2} (1 + \epsilon_{\nu}^{1/2})^{-1} B_{\nu}$, where B_{ν} is the Planck function and $\epsilon_{\nu} = \kappa_{\text{abs},\nu} / (\kappa_{\text{abs},\nu} + \kappa_{\text{es}})$ is the ratio of the absorption to the total opacity, and κ_{es} is the electron scattering opacity. The quantities B_{ν} and ϵ_{ν} are evaluated at the bottom of the thermalization photosphere (TP); we denote the temperature and the density there by T_{ν} and ρ_{ν} , respectively.

The scale height of the photosphere is given by $h_{\nu} \sim [\gamma P_{\text{rad}}(T_{\nu}) / \rho_{\nu}]^{1/2} / \Omega$, where $\gamma \approx 4/3$ is the adiabatic index. We set the absorption opacity equal to the (mainly bound-free) opacity $\kappa_{\nu} \approx 3 \times 10^{26} g_{\text{bf}} \rho T^{-7/2} \xi^{-3} (1 - e^{-\xi}) \text{ cm}^2 \text{ g}^{-1}$ with ρ and T in cgs, where $\xi \equiv h\nu/kT$, h is the Planck constant, and $g_{\text{bf}} \sim 1$ is the gaunt factor (κ_{ν} is the free-free opacity scaled up by the ratio of the bound-free to the free-free Rosseland mean opacities at solar metalicity). By definition, the effective optical depth $\sim (\kappa_{\text{abs},\nu} \kappa_{\text{es}})^{1/2} \rho_{\nu} h_{\nu} = 1$ at the bottom of TP. This is solved for ρ_{ν} , which we substitute back in κ_{abs} to find that $\epsilon_{\nu}^2 = 1.4 \times 10^{42} g_{\text{bf}} \Omega^2 T_{\nu}^{-15/2} \xi^{-3} (1 - e^{-\xi})$. To estimate the degree to which blanketing by the TP modifies the integrated emitted flux, we evaluate ϵ_{ν} at the Wien frequency ($\xi \approx 2.8$). We relate T_{ν} to the midplane temperature via $T_{\nu} = \tau^{-1/4} T$, where τ is the electron-scattering optical depth between the photosphere and the midplane. This yields

$$F_{\text{gb}} \equiv \int_0^{\infty} F_{\nu} d\nu \sim \frac{4\sigma T^4}{3\tau} \frac{\sqrt{\epsilon}}{1 + \sqrt{\epsilon}} \sim \frac{9}{8} \nu \Sigma \Omega^2, \quad (3)$$

where $\epsilon \sim 2.5 \times 10^{20} \Omega \tau^{15/16} T^{-15/4}$ and the last approximate equality in equation (3) follows from identifying F_{gb} with half of the power generated in the disk. The disk edge has $\epsilon < 1$ at decoupling, resulting in a higher midplane temperature than in the black-body disk.

The optical depth is given by $\tau = \theta \kappa \Sigma$, where κ is the opacity (electron-scattering $\kappa_{\text{es}} \approx 0.4 \text{ cm}^2 \text{ g}^{-1}$, or Kramer's $\kappa_{\text{abs}} \approx 1.6 \times 10^{24} \rho T^{-7/2} \text{ g}^{-1}$) and $\theta \leq 1$ is a “porosity” correction factor. We introduce θ to account for the shortened effective optical depth in an inhomogeneous, turbulent disk in which radiation can escape through low-density domains. The correction can also be used to approximate disks in which a significant fraction of the turbulent magnetic energy is dissipated in surface layers (Miller & Stone 2000), or in the presence of photon-bubble instability (Gammie 1998). For example, we estimate that $\theta \approx 0.2$ in Turner (2004).

The surface density is thus far unspecified. One (admittedly artificial) way to parametrize Σ is to fix the accretion rate $\dot{M} \equiv 3\pi\nu\Sigma$ that the disk would have at its inner edge if it contained a single black hole instead of a binary (the disk is not in viscous equilibrium and the accretion rate varies with radius).

TABLE 1. DECOUPLING WITH GREY- AND BLACK-BODY PHOTOSPHERES^a

	α_{-1}	η_{-1}	λ	\dot{m}	M_6	$\beta_{-1}, \frac{4q}{(1+q)^2}$	$\theta_{0.2}$		α_{-1}	η_{-1}	λ	\dot{m}	M_6	$\beta_{-1}, \frac{4q}{(1+q)^2}$	$\theta_{0.2}$	
a/r_g	117	-0.34	0.24	0.70	-0.24	0.08	0.42	-0.08	150	-0.31	0.15	0.54	-0.15	0.08	0.38	-0.08
$T (10^6 \text{ K})$	1.7	0.19	-0.86	-1.95	0.86	-0.28	-0.49	0.30	0.7	0.08	-0.54	-1.38	0.54	-0.27	-0.35	0.27
$t_{\text{sh}} (\text{yr})$	9.4	-1.36	0.98	2.80	-0.98	1.32	1.7, 0.7	-0.34	26	-1.23	0.62	2.15	-0.62	1.31	1.54, 0.54	-0.31
h/r	0.46	0.76	-2.43	-3.80	2.43	-0.12	-0.95	1.19	0.01	0.31	-1.15	-1.54	1.15	-0.08	-0.38	1.08
$P_{\text{rad}}/P_{\text{gas}}$	2600	1.67	-4.25	-7.35	4.25	-0.04	-1.84	2.17	4	0.85	-1.92	-3.23	1.92	0.04	-0.81	1.96
$\kappa_{\text{es}}/\kappa_{\text{abs}}$	46,000	1.76	-4.68	-8.32	4.68	-0.18	-2.08	2.32	15	0.88	-2.19	-3.92	2.19	-0.10	-0.98	2.10
$Q (10^5)$	4.5	2.12	-2.41	-6.61	2.41	-1.44	-1.65	1.53	0.15	1.54	-0.77	-3.69	0.77	-1.38	-0.92	1.38
$Q_{\text{adv}}/Q_{\text{rad}}$	0.44	1.52	-4.86	-7.60	4.86	-0.24	-1.90	2.38	0.0004	0.62	-2.31	-3.08	2.31	-0.15	-0.77	2.15
ϵ	0.0014	-0.84	2.37	4.20	-2.37	0.08	1.05	-0.21	0.04	-0.40	1.14	2.02	-1.14	0.04	0.50	-0.10
$M_{\text{disk}} (M_{\odot})$	96	-1.17	-0.88	-1.15	0.88	2.04	0.21	-0.04	110	-1.15	-0.92	-1.23	0.92	2.04	0.19	-0.04

^aVariable in column 1, defined in the text, equals the factor in column 2 (10) times the product of column head parameters raised to the exponents indicated in columns 3–9 (11–17), where $r_g \equiv GM/c^2$ and we assume $\mu = 0.6$. Parameters on the left side of the separator are for disks with a thermalization, “grey-body” photosphere, the ones on the right side are for black body disks, and all except for M_{disk} are evaluated at the edge of the disk.

The accretion rate can be expressed in units of the Eddington-limited accretion rate $\dot{M}_{\text{edd}} \equiv 4\pi GMm_p/\eta c\sigma_T$, where $\eta \sim 0.1$ is the radiative efficiency and $\sigma_T = m_p\kappa_{\text{es}}$ is the Thomson cross section; \dot{M}_{edd} should not be confused with the *local* Eddington limit at the disk edge. We define the dimensionless parameter $\dot{m} \equiv \dot{M}/\dot{M}_{\text{edd}}$. Note that there is no a priori reason that $\dot{m} \leq 1$. In fact, following decoupling the accretion rate is likely to be the largest anywhere among black holes of the same mass. The surface density is thus parametrized via

$$\nu\Sigma = \frac{4}{3} \frac{GMm_p}{\eta c\sigma_T} \dot{m}. \quad (4)$$

Another way to characterize the surface density is via the total mass of the disk M_{disk} (see Table 1), out to the radius where the temperature falls below 10^4 K (see below).

To determine the disk properties at the time of decoupling, we equate equation (2) to (1), which with the expression for the viscosity, determines the midplane temperature near the disk edge in terms of the semimajor axis a . This is then used in equations (3) and (4) to solve for the semimajor axis a , the edge surface density Σ and the edge midplane temperature T at decoupling. Self-consistent solutions are in the radiation-pressure and electron-scattering dominated regime. The results for disks with grey-body photospheres are summarized on the left of Table 1. We also consider disks with black body photospheres; these results are summarized on the right of Table 1. We have defined $\alpha_{\text{gas}} = 0.1\alpha_{-1}$, $\beta = 0.1\beta_{-1}$, $\eta = 0.1\eta_{-1}$, $M = 10^6 M_6 M_{\odot}$, and $\theta = 0.2\theta_{0.2}$.

We calculate the disk scale height-to-radius ratio $h/r = \Sigma/r\rho$. For the fiducial choice of parameters $\alpha_{-1} = \beta_{-1} = \eta_{-1} = \lambda = \dot{m} = M_6 = q = \theta_{0.2} = 1$, the disk with a grey-body photosphere is marginally geometrically thick at the inner edge, while the black-body disk is geometrically thin. We ignore horizontal and vertical advection but do provide an estimate of the advected-to-radiated heat flux ratio $Q_{\text{adv}}/Q_{\text{rad}}$. Ignoring radiative loss, the advected flux equals $Q_{\text{adv}} = (3/4)(4\gamma_p - 12\gamma_T)\nu\Sigma P_{\text{rad}}/\rho r^2$, where $\gamma_{\rho,T} \equiv d\ln(\rho,T)/d\ln r$; in our disk $(4\gamma_p - 12\gamma_T) \sim 8$. In the fiducial grey-body disk, horizontal advection is competitive with radiative diffusion, implying that the true disk is geometrically thinner than ours, as in the “slim-disk” solutions of Abramowicz et al. (1988).

Just how large could the parameter \dot{m} be? One limit is the requirement that the disk be thin at the edge (h/r)_{edge} $\ll 1$, implying (we ignore the weak dependence on α , M , and μ)

$$\dot{m} \ll \begin{cases} 1.4\beta_{-1}^{0.39}\eta_{-1}\lambda^{1.56}[4q/(1+q)^2]^{0.39}\theta_{0.2}^{-0.49}, & \text{grey body} \\ 42\beta_{-1}^{1/3}\eta_{-1}\lambda^{4/3}[4q/(1+q)^2]^{1/3}\theta_{0.2}^{-14/15}, & \text{black body,} \end{cases} \quad (5)$$

which allows for $\dot{m} \gg 1$ when $q \ll 1$.

A trustworthy disk model should be gravitationally stable, with Toomre (1964) $Q \equiv \Omega^2/\pi G\rho > 1$ throughout. We have checked that the disk structures for $M \leq 10^6 M_{\odot}$ have $Q > 1$ everywhere inside the radius where T falls below 10^4 K and the disks become susceptible to ionization instability. We do not extrapolate our disks beyond this point.

3. DETECTION OF THE ELECTROMAGNETIC AFTERGLOW

Following decoupling, the binary proceeds to coalescence in time $t_{\text{gr}}/4$, where t_{gr} is evaluated at decoupling, while the inner edge of the accretion disk migrates inward on time scale $\sim t_{\text{sh}} \sim t_{\text{gr}}$. Therefore, in time $\sim (3/4)t_{\text{sh}}$, the inner edge arrives at the now-coalesced black hole. The arrival is accompanied by rapid accretion and the activation of an X-ray AGN. The pre-coalescent circumbinary disk is expected to be luminous in IR with a negligible X-ray counterpart. The IR source, however, may be confused with the light of the host galaxy. Barth et al. (2004) recently studied the dwarf galaxy POX 52, which appears to contain a $1.6 \times 10^5 M_{\odot}$ black hole accreting at about the Eddington rate (see also Greene & Ho 2004 for other such candidates). The optical luminosity of the POX 52 black hole is about the same as that of the galaxy.

The coalescence may be accompanied by radiation-recoil (e.g., Merritt et al. 2004, and references therein). The velocity of the recoiled black hole $\lesssim 300 \text{ km s}^{-1}$, however, is smaller than the orbital velocity of the disk at the inner edge $\sim (2-3) \times 10^3 \text{ km s}^{-1}$. The inner disk remains bound and the afterglow is hardly affected.

Since the coalescence of a pair of black holes with masses $10^{5-7}(1+z)^{-1}M_{\odot}$ at redshifts $z \lesssim 20$ will be detected by LISA at high signal-to-noise, it is natural to ask whether the burst of GR and its electromagnetic afterglow may be detected in succession. We use Table 1 to estimate the observed interval $\Delta t \sim (3/4)(1+z)t_{\text{sh}}$ between the two signals. For example, for the merger of two $10^5 M_{\odot}$ black holes at redshift $z = 5$, assuming that $\alpha_{-1} = \beta_{-1} = \eta_{-1} = \dot{m} = \theta_{0.2} = 1$, we find $\Delta t \sim 2 \text{ yr}$ for a grey-body disk truncated at $r_{\text{edge}} = 2a$.

The *James Webb Space Telescope* (JWST) will have greatest sensitivity between $\sim (1-4)\mu\text{m}$.³ Therefore, wavelengths from mid-UV to near-IR emitted at $z \lesssim 20$ can contribute to the signal detected by JWST. Most of this radiation comes from radii in the disk exterior to the inner edge at decoupling (see Figure 1). Therefore, the post-coalescence IR-optical

³ <http://www.stsci.edu/jwst>

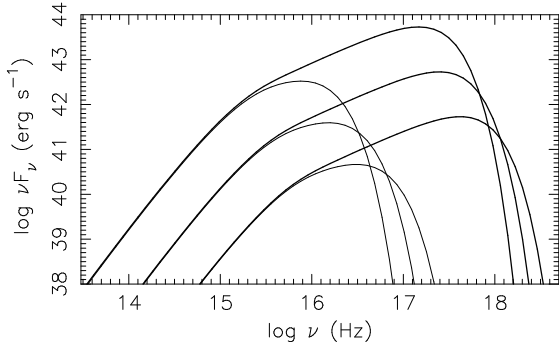


FIG. 1.— Thermal modified black-body spectra of Eddington-limited ($\dot{m} = 1$) accretion disks around black holes of mass $M = (10^4, 10^5, 10^6) M_{\odot}$ (thick lines, from right to left) and dimensionless spin parameter $a_* = 0.9$ (we ignored Doppler broadening). Only the emission from rings in the disk with $r < 1000 r_g$ was taken into account. These crude spectra are compatible with detailed models of Hubeny et al. (2001). We also show disk spectra at the moment of binary-disk decoupling, as discussed in § 2 (thin lines).

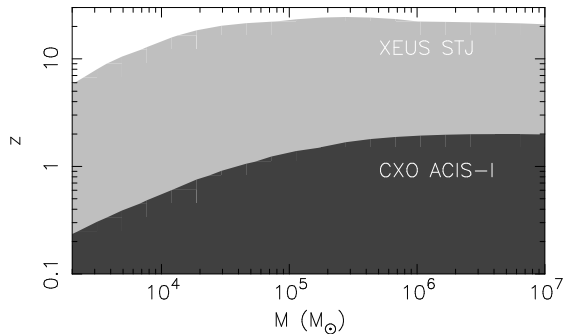


FIG. 2.— Redshifts at which emission from an Eddington-accreting ($\dot{m} = 1$) black hole of mass M can be detected with 10^5 exposure using the instrument ACIS-I on *Chandra* (dark-grey) and the Hafnium superconducting tunneling junction (STJ) detector on XEUS before mission upgrade (light-grey). We assume that ten counts constitute detection and ignore absorption and confusion. The disk spectra were thermal modified black-body spectra for a nearly-maximally spinning black hole, $a_* = 0.9$. We assume the standard Λ CDM cosmology with $H_0 = 70 \text{ km s}^{-1} \text{ Mpc}^{-1}$, $\Omega_m = 0.3$ and $\Omega_{\Lambda} = 0.7$.

flux will not differ significantly from the pre-coalescence flux. One exception would be if the merged black hole were completely enshrouded by a large column depth of gas and dust. Then, the UV–X-ray emission of the afterglow would be re-processed to longer wavelengths, and such shrouded merger could be identified by a sudden increase in IR luminosity.

The arrival of the inner edge of the accretion disk at the black hole will be accompanied by a sudden activation of X-ray emission from a rapidly-accreting AGN. Most of the luminosity of the post-coalescent accretion disk around a $(10^4 - 10^6) M_{\odot}$ black hole is emitted at rest-frame energies $h\nu \sim (0.5 - 5) \text{ keV}$, which fall within the sensitivity windows of future X-ray detectors such as XEUS⁴ and *Generation-X*⁵. XEUS could see this emission at $z \sim 20$ for $(10^5 - 10^6) M_{\odot}$ black holes. For smaller black hole masses the maximum redshift for detection decreases with the decreasing mass (see Figure 2).

We propose that location with detected GR signals from MBH coalescence be monitored in the $0.1 - 10 \text{ keV}$ band at high angular resolution. The angular resolution of LISA ranges from several arcminutes to several degrees depending on the black hole mass, mass ratio and redshift (Cutler 1998; Hughes 2002). Therefore multiple exposures of an X-ray telescope may be necessary for some sources. A possibly confusing source of X-ray flares are tidal disruptions of main sequence stars (Rees 1990; Cannizzo, Lee, & Goodman 1990; Komossa et al. 2004).

Detection of the afterglow of MBH coalescence will help pinpoint the location and hence redshift of GR sources. The detailed light curve of the afterglow will probe the structure of the accretion disk as it moves to toward the black hole, and will also shed light on the cosmological assembly of MBHs.

We thank Aaron Barth and Tom Prince for valuable discussions. M. M. was supported at Caltech by a postdoctoral fellowship from the Sherman Fairchild Foundation. E. S. P. was supported in part by NASA ATP grants NAG5-10707 and NNG04GK98G.

⁴ <http://www.rssd.esa.int/index.php?project=XEUS>

⁵ <http://generation-x.gsfc.nasa.gov>

REFERENCES

Abramowicz, M. A., Czerny, B., Lasota, J. P., & Szuszkiewicz, E. 1988, *ApJ*, 332, 646

Armitage, P. J. & Natarajan, P. 2002, *ApJ*, 567, L9

Artymowicz, P. & Lubow, S. H. 1994, *ApJ*, 421, 651

Artymowicz, P. & Lubow, S. H. 1996, *ApJ*, 467, L77

Balbus, S. A. & Hawley, J. F. 1991, *ApJ*, 376, 214

Bardeen, J. M. & Petterson, J. A. 1975, *ApJ*, 195, L65

Barth, A. J., Ho, L. C., Rutledge, R. E., & Sargent, W. L. W. 2004, *ApJ*, 607, 90

Begelman, M. C. 2002, *ApJ*, 568, L97

Begelman, M. C., Blandford, R. D., & Rees, M. J. 1980, *Nature*, 287, 307

Cannizzo, J. K., Lee, H. M., & Goodman, J. 1990, *ApJ*, 351, 38

Cutler, C. 1998, *Phys. Rev. D*, 57, 7089

Gammie, C. F. 1998, *MNRAS*, 297, 929

Greene, J. E. & Ho, L. C. 2004, *ApJ*, 610, 722

Greenhill, L. J., et al. 2003, *ApJ*, 590, 162

Hubeny, T., Blaes, O., Krolik, J. H., & Agol, E. 2001, *ApJ*, 559, 680

Hughes, S. A. 2002, *MNRAS*, 331, 805

Ivanov, P. B., Papaloizou, J. C. B., & Polnarev, A. G. 1999, *MNRAS*, 307, 79

Jackson, J. M., Geis, N., Genzel, R., Harris, A. I., Madden, S., Poglitsch, A., Stacey, G. J., & Townes, C. H. 1993, *ApJ*, 402, 173

Komossa, S., Halpern, J., Schartel, N., Hasinger, G., Santos-Lleo, M., & Predehl, P. 2004, *ApJ*, 603, L17

Larwood, J. D. & Papaloizou, J. C. B. 1997, *MNRAS*, 285, 288

Lightman, A. P. & Eardley, D. M. 1974, *ApJ*, 187, L1

Lynden-Bell, D. & Pringle, J. E. 1974, *MNRAS*, 168, 603

Merritt, D., Milosavljević, M., Favata, M., Hughes, S. A., & Holz, D. E. 2004, *ApJ*, 607, L9

Miller, K. A. & Stone, J. M. 200, *ApJ*, 534, 398

Milosavljević, M. & Merritt, D. 2003, *ApJ*, 596, 860

Miyoshi, M., Moran, J., Herrnstein, J., Greenhill, L., Nakai, N., Diamond, P., & Inoue, M. 1995, *Nature*, 373, 127

Peters, P. C. 1964, *Physical Review*, 136, 1224

Rees, M. J. 1990, *Science*, 247, 817

Sakimoto, P. J. & Coroniti, F. V. 1981, *ApJ*, 247, 19

Shakura, N. I. & Sunyaev, R. A. 1973, *A&A*, 24, 337

Toomre, A. 1964, *ApJ*, 139, 1217

Turner, N. J. 2004, *ApJ*, 605, L45

Turner, N. J., Stone, J. M., Krolik, J. H., & Sano, T. 2003, *ApJ*, 593, 992